PERGAMON

International Journal of Heat and Mass Transfer 43 (2000) 3497–3509

International Journal of HEAT and MASS TRANSFER

www.elsevier.com/locate/ijhmt

Technical Note

The effect of nozzle configuration on stagnation region heat transfer enhancement of axisymmetric jet impingement

Jungho Lee, Sang-Joon Lee*

Department of Mechanical Engineering, Advanced Fluids Engineering Research Center, Pohang University of Science and Technology, San 31, Hyoja-dong, Pohang 790-784, South Korea

Received 3 May 1999; received in revised form 23 September 1999

1. Introduction

Impinging jet heat transfer has been established as an effective technique for heating, cooling, or drying a target surface and has a variety of engineering applications. Many previous investigations have been carried out to understand the heat and mass transfer characteristics of impinging jet through experiments and numerical calculations [1,2].

There have been a few studies which investigated the effects of nozzle configurations on the impinging jet heat transfer. Gardon and Akfirat [3] investigated the flow and heat transfer characteristics of two-dimensional and axisymmetric impinging jets. Hoogendoorn [4] studied the effect of flow turbulence on the stagnation heat transfer of impinging jets issuing from both a long straight pipe and a smoothly convergent nozzle. Obot et al. [5] investigated the effects of three different nozzle geometries on the flow and heat transfer characteristics of round impinging jets, which focused on the nozzle length-to-diameter ratio. Popiel and Boguslawski [6] showed that the nozzle exit configuration is the most important factor affecting the stagnation point heat transfer. Pan et al. [7] investigated the effects of nozzle configuration on the stagnation region heat transfer of axisymmetric free surface liquid impinging jets. Oyakawa et al. [8] measured the local and average heat transfer for three square-edged orifice nozzles with different cross-sections; round, elliptic and cross-shaped.

The objective of this study is to understand the effects of nozzle exit configurations on the heat transfer enhancement of an axisymmetric impinging orifice jet in the stagnation region. Three different orifice nozzles having the same exit diameter D; (1) sharp-edged orifice nozzle, (2) standard-edged orifice nozzle, and (3) square-edged orifice nozzle, were tested for the nozzle-to-plate spacings of $L/D = 2$, 4, 6 and 10. The jet Reynolds numbers were ranged from 5,000 to 30,000. A relatively large nozzle diameter of $D = 25$ mm and the liquid crystal thermometry technique were employed in this study to achieve better spatial resolution in the stagnation region heat transfer measurement. As the heat transfer rate on the impingement surface has a close relationship with the momentum transfer rate of the impinging jet, velocity measurements at the nozzle exit were also performed to get a better understanding on the heat transfer characteristics with respect to nozzle configuration.

2. Experimental apparatus and analysis

The experimental apparatus consists of an axial blower, a heat exchanger, a honeycomb, screens, an orifice flowmeter, a long straight pipe and a heated impingement plate. The air flow rate was measured with an ASME standard orifice flowmeter. The

* Corresponding author. Tel.: +82-562-279-2169; fax: +82-562-279-3199.

E-mail addresses: jupi@postech.ac.kr (J. Lee), sjlee@postech.ac.kr (S.-J. Lee).

0017-9310/00/$ - see front matter
PII: S0017-9310(99)00349-X

Nomenclature

D	nozzle exit diameter
h	local heat transfer coefficient, Eq. (1)
k	thermal conductivity of air
L	distance between nozzle exit and impingement plate
L/D	dimensionless nozzle-to-plate spacing
Nu	local Nusselt number, Eq. (1)
Nu_0	stagnation point Nusselt number
$\overline{Nu}$	average Nusselt number, Eq. (2)
q_v	convection heat flux
R	radial distance from the stagnation point
R/D	dimensionless radial distance from the stagnation point *Re* Reynolds number based on the nozzle exit diameter, ($\equiv U_e D/\nu$)
T_j	jet exit temperature
T_w	local wall temperature (liquid crystal temperature on heated surface)
t	thickness of orifice nozzle
u'_c	fluctuating streamwise velocity at nozzle centerline
U_c	mean streamwise velocity on the jet centerline
U_e	mean velocity at the nozzle exit
Z	axial distance from the nozzle exit along jet centerline
Z/D	dimensionless axial distance from the nozzle exit

Greek symbols

ε	emissivity of liquid crystal coating
σ	Stefan–Boltzmann constant
ν	kinematic viscosity of air

heated impingement plate is composed of Plexiglas, gold-coated film and thermochromic liquid crystal. A transparent gold-coated film of 127 μm thick, 20 × 15 cm in size was glued on the Plexiglas plate of 30.3 × 30.3 cm to provide a nearly constant heat flux on the heated plate. A black backing paint and a thermochromic liquid crystal (TLC) were uniformly sprayed on the back side of the gold-coated film. The combined thickness of the TLC and black paint was about 60 μm. The liquid crystal used in present study was 'R35C1W' microencapsulated TLC purchased from Hallcrest. An image processing system was used to quantitatively determine the surface temperature corresponding to isothermal contours of liquid crystal. The experimental apparatus and the digital image processing system used in this study are described in detail by Lee and Lee [9,10].

Fig. 1 shows three orifice nozzles having different exit configuration tested in this study; (1) sharp-edged orifice nozzle, (2) standard-edged orifice nozzle and (3) square-edged orifice nozzle were attached at the pipe end. All nozzles have the same exit diameter of $D = 25$ mm and the same nozzle length-to-diameter ratio of $t/D = 0.2$. Each orifice nozzle was attached at the end of the long straight PVC pipe with an internal diameter of 52.3 mm and length of 2.5 m.

Since the impingement surface has constant heat flux, an isotherm on the impingement surface corresponds to a contour of constant heat transfer coefficient. As the heat flux input changes, the isothermal contour is also changed according to the energy balance. The local convective heat transfer coefficient was calculated from

$$h = \frac{q_v}{T_w - T_j} \quad \text{and } Nu = \frac{hD}{k} \tag{1}$$

where convective heat flux q_v is obtained by subtracting the energy losses from the total imposed heat flux input through the gold-coated film. In present study, the thermal entrainment effects of ambient air were minimized by maintaining the impinging air jet temperature as close as the ambient temperature for all experiments ($T_a - T_j = \pm 0.1^\circ C$). Therefore, the jet exit temperature was used to calculate the local heat transfer coefficient instead of the local adiabatic wall temperature. The wall temperature T_w was measured by tracing the red-to-yellow color transition of liquid crystal on the heated flat plate. The spatial resolution in determining the isotherm was estimated to be 0.3 ± 0.05 mm. The TLC calibration results showed that the isotherm for the red-to-yellow color transition was 34.8 ± 0.15°C. More detailed heat transfer measurement procedures are described by Lee [11].

The local Nusselt number distribution was averaged to obtain an average Nusselt number. The average Nusselt number is defined as

$$\overline{Nu} = \bar{h}\frac{D}{k} = \frac{2}{R^2}\int_0^R Nu(r)\,\mathrm{d}r \tag{2}$$

The integral equation was calculated using the Newton–Cotes formula with three-point correlation based on measured local Nusselt numbers.

The uncertainty of local Nusselt numbers measured in this study has been evaluated for all experimental arrangements and procedures using the 20:1 odds method suggested by Kline and McClintock [12]. The total uncertainty of the local Nusselt numbers was ran-

ged from 3.02 to 5.79%. The nonuniformity factor of gold coating was the largest contributor to the total uncertainty and its uncertainty was ranged from 2.17 to 4.13%. Another important source of uncertainty was the wall temperature T_w of which the uncertainty was in the range of 1.57–3.98%. The average Nusselt number $\overline{Nu}$ has uncertainty in the range of 3.80–6.53%. The uncertainties in the Reynolds number calculation and the radial position (R/D) determination on the plate were estimated to be within 2.0–4.5% and 0.8%, respectively.

A single hot-wire probe (Dantec 55P11) was used to measure the streamwise mean velocity (U) and turbulence intensity ($((\overline{u'}^2)^{1/2}/U_e)$). The hot-wire probe was connected to a constant temperature anemometer (TSI IFA-100). The analog velocity signal from the anemometer was digitized at 2 kHz sampling rate for 10 s by an A/D converter (DT2838) after 800 Hz low-pass filtering. Then the mean velocity and turbulence intensity were obtained statistically. The uncertainties of the measured mean velocity and turbulence intensity were estimated to be less than 1.5 and 3.5%, respectively.

3. Results and discussion

The mean velocity decay and turbulence intensity measured along the jet centerline of three different orifice nozzles are compared in Fig. 2. The centerline mean velocity decay is suddenly decreased from the nozzle exit and the jet potential core exists up to $Z/D \cong 4$. This sudden decrease is strongly attributed to the vena contracta that commonly encountered in orifice jets. At $Z/D \cong 0.5$, all orifice jets show initial rapid increase and subsequent decrease of the centerline velocity. It should be also mentioned that the mean velocity decay for the sharp-edged orifice jet is larger than the other jets. The turbulence intensity distribution measured along the jet centerline shows a gradual increase with going downstream and obtains a peak value at $Z/D \cong 7$. Behind the locations of maximum turbulence intensity, the velocity fluctuations gradually decrease. The maximum turbulence intensity for the sharp-edged orifice nozzle case is higher than the other two nozzles. The sharp-edged orifice nozzle produces a thin momentum thickness, causing strong

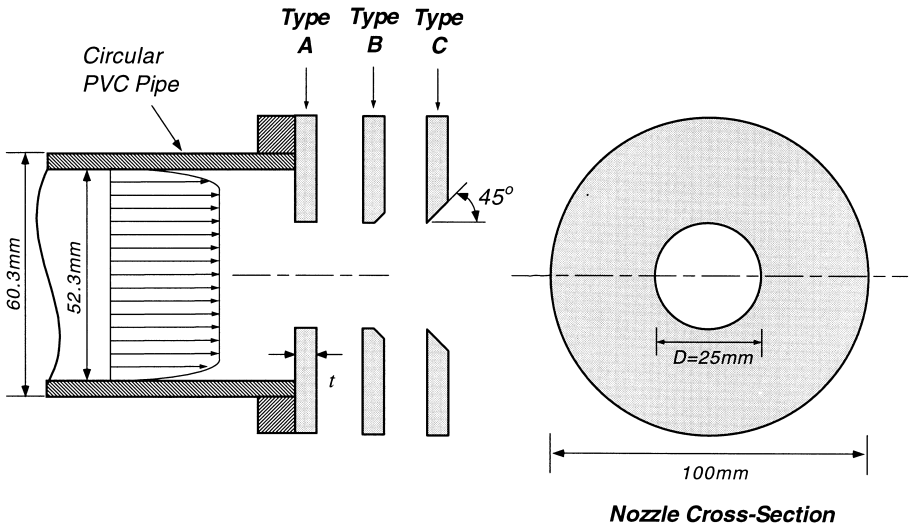

Nozzle exit diameter of D = 25 mm

Nozzle Type	Nozzle Name	t	t/D
A	Square-edged orifice	5	0.2
B	Standard-edged orifice		
C	Sharp-edged orifice		

Fig. 1. Configuration of orifice nozzles tested in this study.

azimuthal variations and large entrainment before the vortical structure is diffused by viscosity [13,14]. Fig. 3 shows the mean velocity and turbulence intensity profiles at the nozzle exit plane ($Z/D = 0$). The mean velocity and turbulence intensity profiles have a nearly top-hat shape, except the edge side of the nozzle. The mean velocity and turbulence intensity profiles have peak values in the nozzle exit plane at $R/D \cong 0.38$, 0.40 and 0.45, for the sharp-edged, standard-edged and square-edged orifice nozzle, respectively. The difference in the peak location results from the intrinsic flow characteristics related with different nozzle configurations. The sharp-edged orifice nozzle causes more vigorous turbulence behaviors, compared to the other two orifice jets.

The effects of nozzle configurations on the stagna-

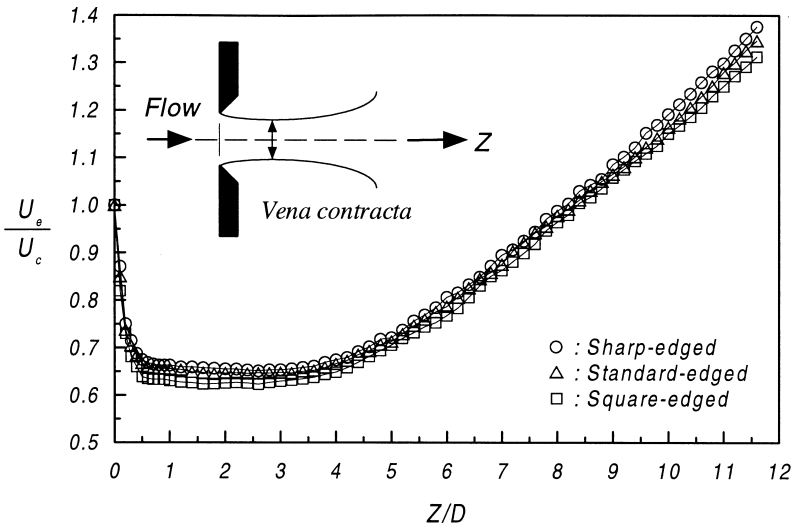

(a) Mean velocity decay

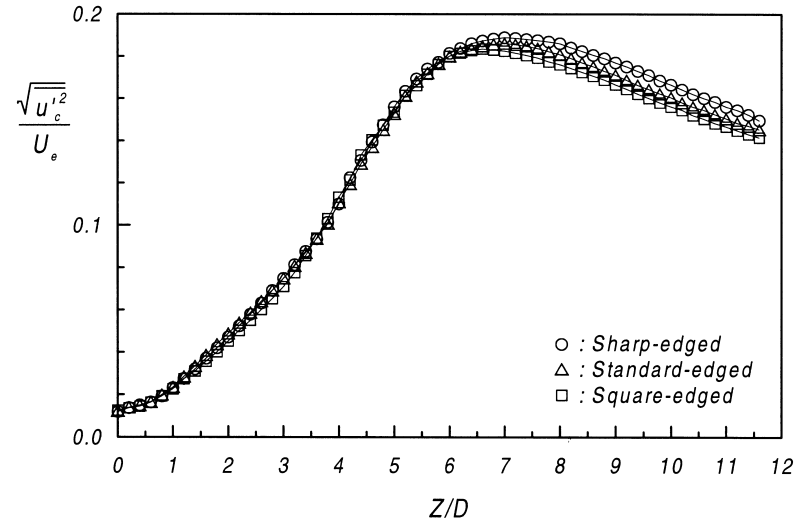

(b) Turbulence intensity

Fig. 2. Mean velocity decay and turbulence intensity measured along the jet centerline at $Re = 10{,}000$.

tion point heat transfer are shown in Fig. 4 as a function of jet Reynolds number. At $L/D = 2$, the stagnation Nusselt number varies according to $Nu_0 \propto Re^{0.54}$, $Re^{0.52}$ and $Re^{0.51}$, for the sharp-edged, standard-edged and square-edged orifice nozzle, respectively. These results nearly agree with the laminar boundary layer flow case [1]. The Reynolds number dependency of the sharp-edged orifice is larger than that of the other two jets. The effect of nozzle exit configuration on the stagnation point heat transfer is more sensible at shorter nozzle-to-plate spacing. With increasing the nozzle-to-plate spacing, the Reynolds number dependence becomes stronger. Comparative results of the contoured nozzle [3] and fully-developed pipe nozzle [9] at $L/D = 2$ are also included. The present Nu_0 data (orifice nozzle jet) for $L/D = 2$ are about 25–55% higher than the fully-developed pipe jet [9] and approximately 50–75% higher than the contoured jet [3]. These heat

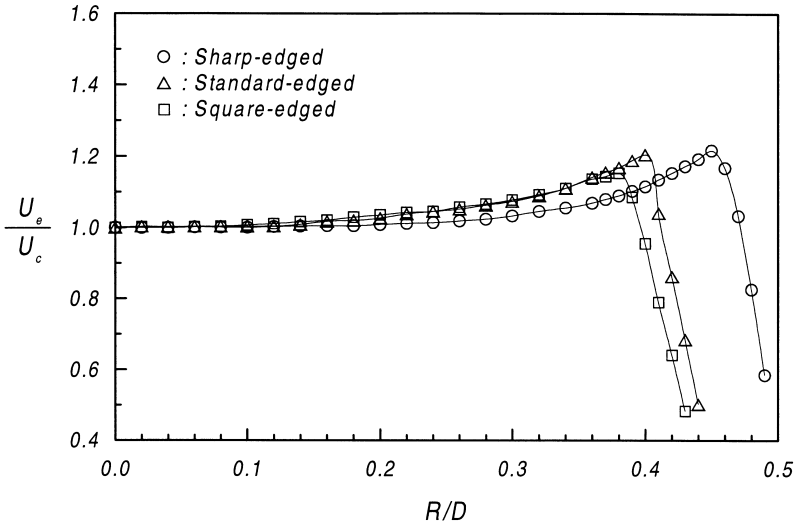

(a) Mean velocity

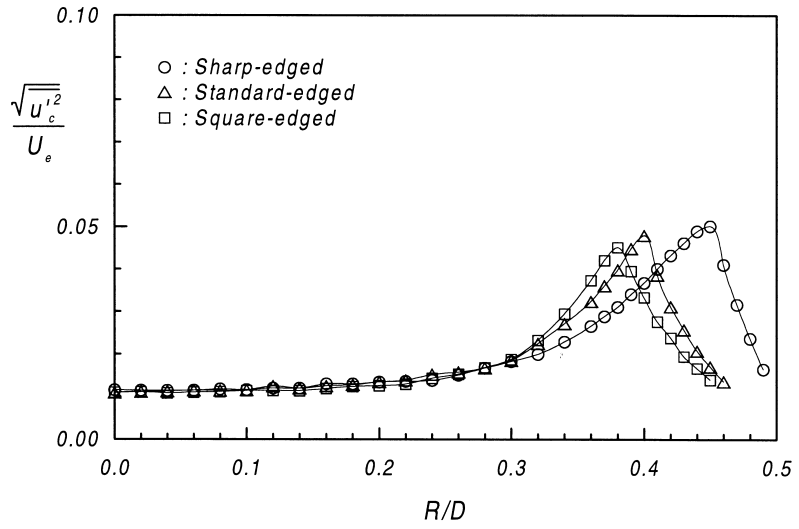

(b) Turbulence intensity

Fig. 3. Mean velocity and turbulence intensity profiles at the nozzle exits for $Re = 10{,}000$.

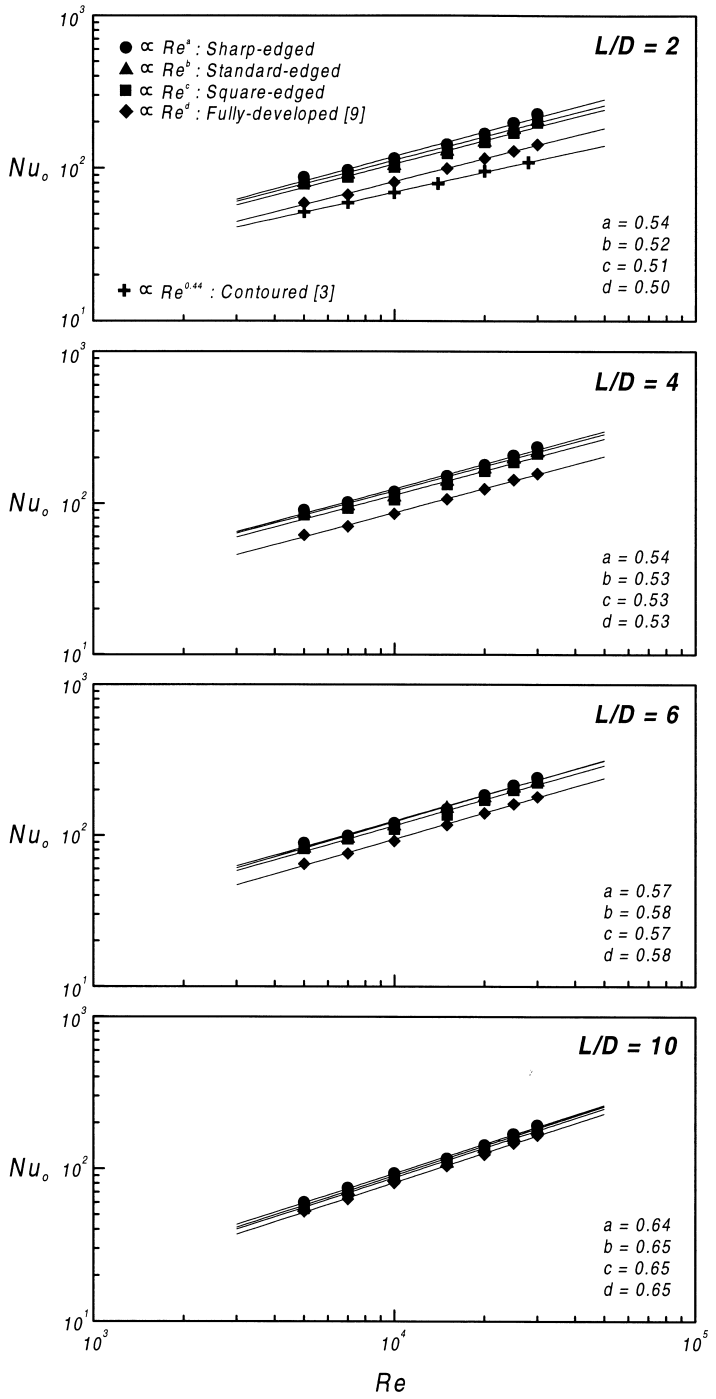

Fig. 4. Reynolds number dependency of stagnation Nusselt numbers at the nozzle-to-plate spacings of $L/D = 2$, 4, 6, and 10.

transfer enhancements are attributed to the larger velocity gradient and higher turbulence intensity of the orifice jets. As the nozzle-to-plate spacing increases beyond the potential core ($\cong$4D), the exponents of Reynolds number become nearly equivalent. Note that while the stagnation point heat transfer rate is sensitive to the nozzle exit configuration for small nozzle-to-plate spacings, the subsequent invariance on the Reynolds number exponent is exhibited at large nozzle-to-plate spacing.

For all tested experimental data, the stagnation point Nusselt numbers are correlated with the jet Rey-

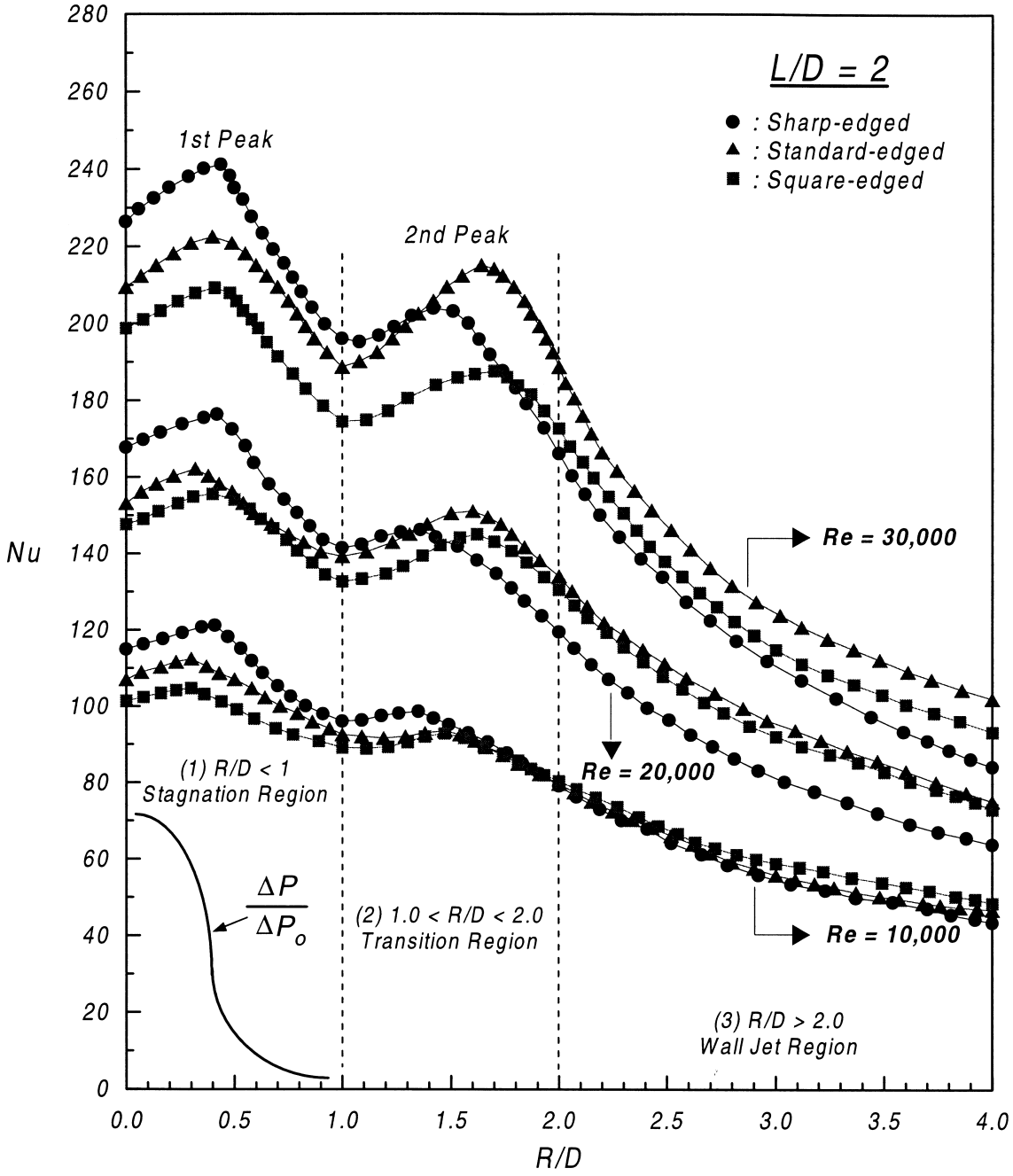

Fig. 5. Local Nusslet number distribution at the nozzle-to-plate spacing of $L/D = 2$.

nolds number Re and nozzle-to-plate spacing L/D. The least-square curve fittings of the stagnation point heat transfer data have following correlations

$$Nu_0 = 0.698 Re^{0.573} (L/D)^{-0.116}: \quad \text{sharp-edged orifice} \tag{3}$$

$$Nu_0 = 0.661 Re^{0.571} (L/D)^{-0.092}: \quad \text{standard-edged orifice} \tag{4}$$

$$Nu_0 = 0.641 Re^{0.566} (L/D)^{-0.078}: \quad \text{square-edged orifice} \tag{5}$$

The Reynolds number dependence ($Nu_0 \propto Re^{0.573}$) for the sharp-edged orifice jet is stronger than the other two jets. Thus, the sharp-edged orifice nozzle is more favorable on the heat transfer enhancements at the stagnation point than any other nozzle configurations.

The local Nusselt number distributions for $L/D = 2$ are shown in Fig. 5. The local Nusselt numbers at the first peaks (Nu_{1st}) are approximately 3.3–6.5% higher than the stagnation point values (Nu_0) and their ratios (Nu_{1st}/Nu_0) are nearly invariant with increasing the jet Reynolds number. The first peak values of the sharp-edged orifice jet are about 5–6% higher than the stagnation point values. This correspondingly coincides with the result of Pan et al. [7]. However, the local Nusselt numbers at the second peaks (Nu_{2nd}) are approximately 2–14% less than the stagnation point values. The Nusselt number ratio of the second peak to the stagnation point value (Nu_{2nd}/Nu_0) is decreased with increasing the jet Reynolds number contrary to the ratio of Nu_{1st}/Nu_0. The ratio of Nu_{2nd}/Nu_{1st} is weakly dependent on the jet Reynolds number. These results indicate that the heat transfer mechanism between these two peaks is nearly independent of the jet Reynolds number.

The first peaks in local Nusselt number distributions corresponding to the maximum heat transfer rates occur at the vicinity of lateral edge ($R/D \cong 0.5$) of the orifice nozzles. The first peak is strongly attributed to the high turbulence intensity at the nozzle edge. For the case of sharp-edged orifice jet, the first peak location ($R/D \cong 0.45$) is well agreed with the velocity data shown in Fig. 3. The large-scale toroidal vortices strike the impingement plate at which the heat transfer rates have the local maximum [10]. The secondary peaks occur in the range of $1.35 \leq R/D \leq 1.7$ for all nozzle configurations and Reynolds numbers tested. With increasing the Reynolds number, the location of the secondary peak moves outward in the radial direction and the peak values are also increased. For the sharp-edged orifice nozzle, the secondary peak is located at $R/D \cong 1.4$ and this agrees approximately with the location of induced interacting toroidal vortices as shown in Lee and Lee [10].

From these results, we can conjecture that the secondary peak was attributed to the transition from laminar to turbulent boundary layer in the spreading wall jet as suggested by Gardon and Akfirat [3]. This transition seems to be triggered by disappearance of pressure gradient which exists in the stagnation region. The pressure gradient serves to stabilize the laminar boundary layer, despite of high turbulence levels in the free jet stream [15]. For the case of standard-edged and square-edged orifice nozzle, the secondary peaks are located a little downstream locations ($R/D \cong$ 1.5–1.7) compared to the sharp-edged orifice nozzle ($R/D \cong 1.4$). This is mainly caused by the fact that the boundary layer transition of the sharp-edged orifice jet occurs ahead of the other two jets inside the transition region. This is also closely related with the fact that the velocity decay rate of the sharp-edged orifice jet is faster than the other two jets as shown in Fig. 2. Thus, in the wall jet region, the heat transfer rates of the sharp-edged orifice are smaller than those of the other two jets.

The local heat transfer distributions for the nozzle-to-plate spacing of $L/D = 6$ are shown in Fig. 6. The local Nusselt numbers decrease monotonically and do not show the secondary maxima at all. Both the sharp-edged and standard-edged orifice jets, the local heat transfer distributions show nearly similar shapes in the wall jet region. The off-stagnation peak is still apparent and the maximum heat transfer rates occur at $R/D \cong$ 0.1. In the stagnation region, the sharp-edged orifice jet has higher heat transfer rates than the other two jets. The stagnation point Nusselt numbers of the sharp-edged orifice jet are approximately 7–9% higher than those of the square-edged orifice jet. However, in the transition and wall jet regions, the local heat transfer rates of the square-edged orifice jet are higher than the sharp-edged and standard-edged orifice jet. The maximum heat transfer rate occurs in the stagnation region for the nozzle-to-plate spacing of $L/D = 6$, irrespective of the jet Reynolds number. This attributes to the highest turbulent intensity of impinging jet near $L/D = 6$ as shown in Fig. 2.

The local Nusselt number distributions for different nozzle configurations at Reynolds number of 20,000 are compared in Fig. 7. Fig. 7(a) shows the effect of nozzle configuration on local heat transfer rates at $L/D = 2$. The results for the fully developed pipe jet [9] and contoured jet [3] at the same Reynolds number are included for comparison. The stagnation point heat transfer rate of the sharp-edged orifice nozzle is 9.5, 13.6, 45.2 and 73.7% higher than that of the standard-edged orifice, square-edged orifice, fully-devel-

oped pipe and contoured nozzle, respectively. Among these nozzle configurations, the sharp-edged orifice nozzle was found to be the most effective for enhancing the local heat transfer rate in the stagnation region. Fig. 7(b) represents the local heat transfer rate distributions at $L/D = 10$. The present Nusselt number distributions of orifice jets are compared with those for the fully developed pipe jet [9] and squared-edged orifice jet with $t/D = 1.0$ [16]. The stagnation point Nusselt number of the sharp-edged orifice jet is about 1.9,

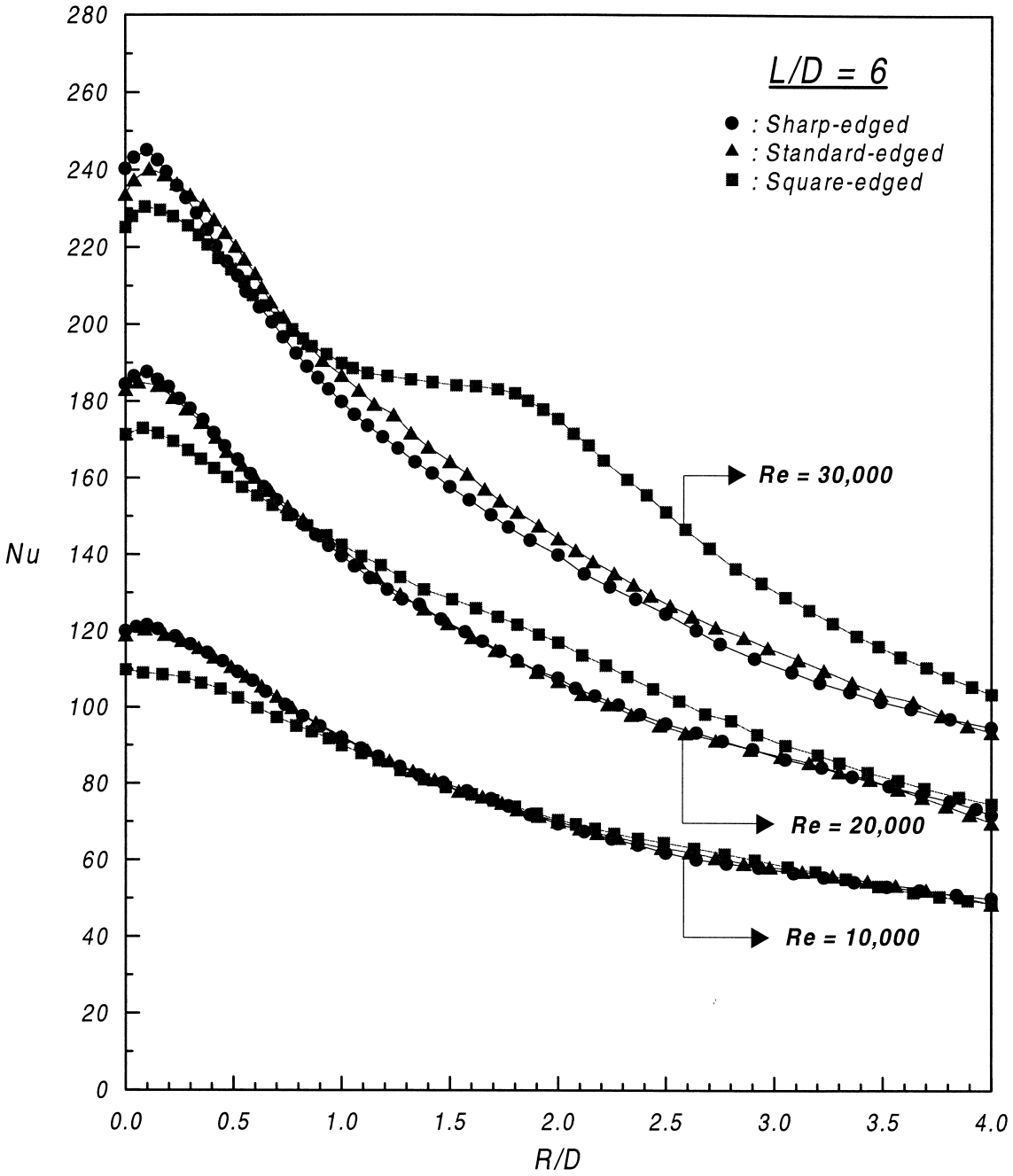

Fig. 6. Local Nusslet number distribution at the nozzle-to-plate spacing of $L/D = 6$.

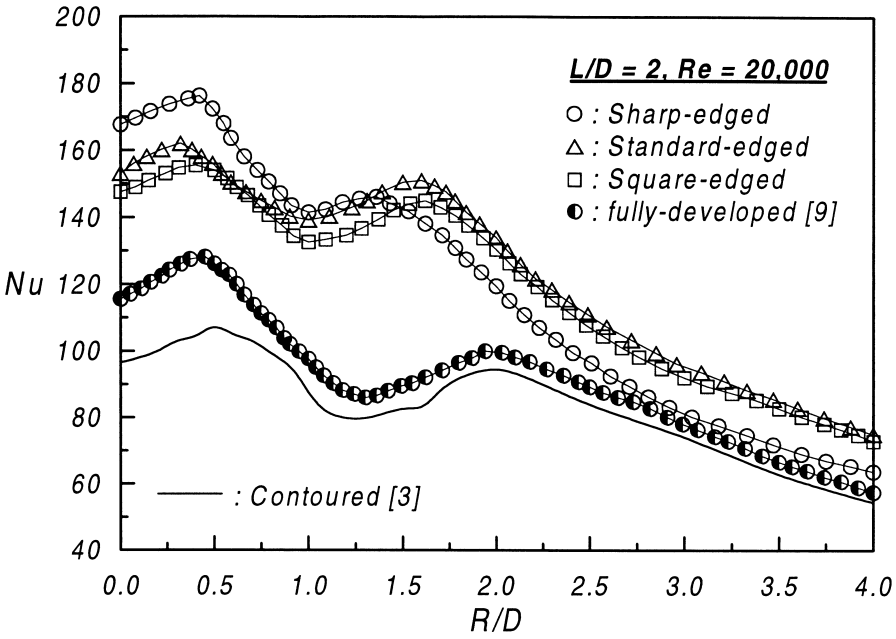

(a) $L/D = 2$ for $Re = 20{,}000$

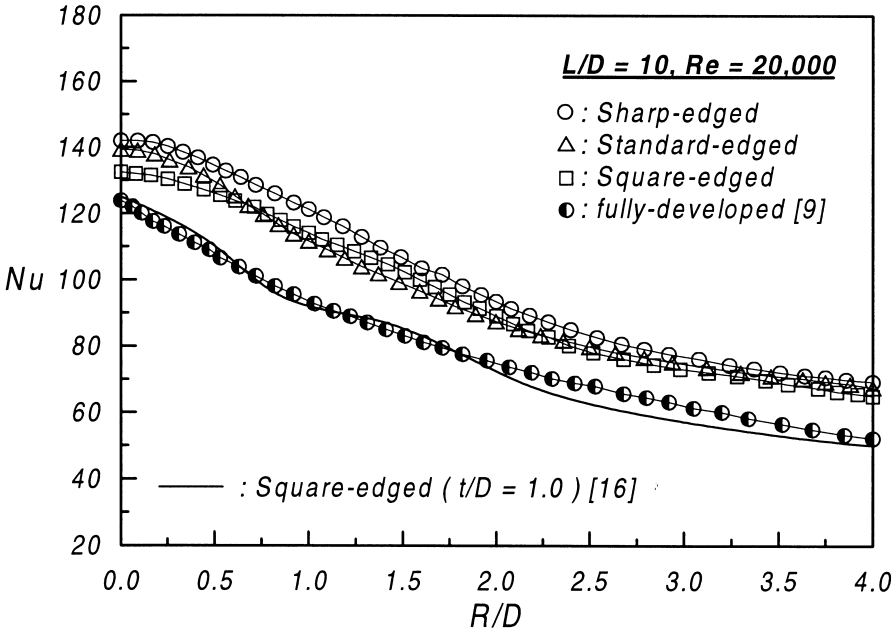

(b) $L/D = 10$ for $Re = 20{,}000$

Fig. 7. Effects of nozzle configuration on local Nusselt number distributions at $Re = 20{,}000$.

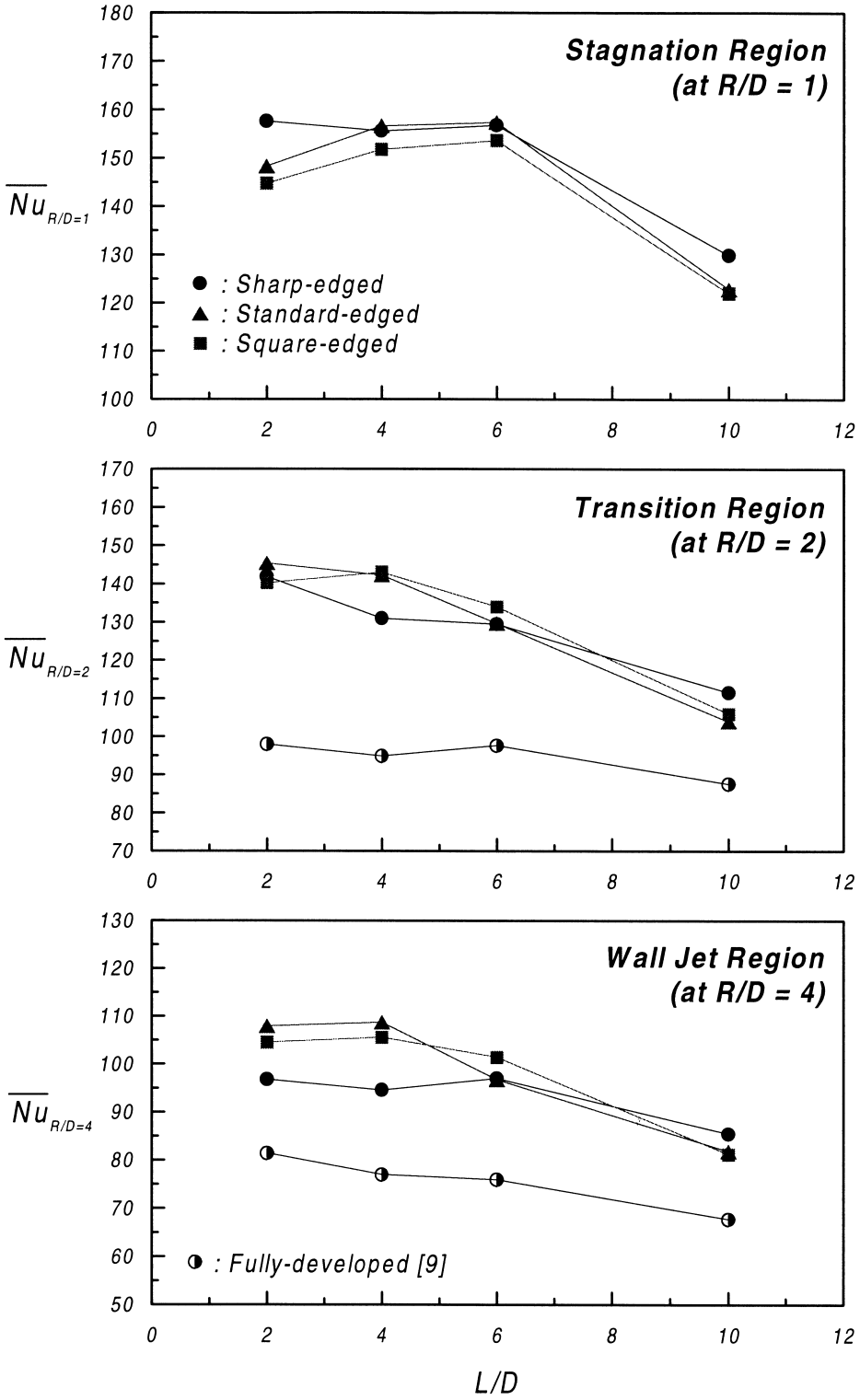

Fig. 8. Variations of average Nusselt numbers with nozzle-to-plate spacing at $Re = 20{,}000$.

7.2, 13.6 and 14.7% higher than that of the standard-edged orifice, square-edged orifice with $t/D = 0.2$ and 1.0 [16], and fully-developed pipe nozzle, respectively. The influence of nozzle configuration on local heat transfer rates is significantly decreased, compared to the case of $L/D = 2$. However, the orifice jets tested in this study give still higher heat transfer rates than the fully-developed pipe jet. This indicates that the nozzle configuration affects the velocity profile at the nozzle exit and the toroidal vortices around the jet circumference consecutively influence the local heat transfer rate.

The average Nusselt numbers for the three regions of $R/D = 1.0$, 2.0 and 4.0 at jet Reynolds number of 20,000 are shown in Fig. 8. In the stagnation region ($R/D < 1.0$), the average heat transfer rate of the sharp-edged orifice jet is about 9% higher than that of the square-edged orifice jet at $L/D = 2$. For the other nozzle-to-plate spacings, the sharp-edged orifice jet gives also higher values than the square-edged orifice jet. This indicates that the sharp-edged orifice nozzle is useful for heat transfer enhancement in the stagnation region. In the transition and wall jet region, the average heat transfer rates decrease with increasing the nozzle-to-plate spacings due to the boundary layer transition on the impingement surface. At $L/D = 2$, the average heat transfer rate for three orifice nozzles is about 40% higher than that of the fully developed pipe nozzle in the transition region. The difference in the average heat transfer rate between the orifice nozzles and the fully-developed pipe nozzle is decreased with increasing L/D. In the wall jet region, the average heat transfer rate of the standard-edged orifice jet is 12 and 40% higher than that of the sharp-edged orifice and fully-developed jet at $L/D = 2$. This attributes to the fact that the sharp-edged orifice jet experiences the boundary layer transition earlier than the square-edged orifice, and consequently has relatively smaller heat transfer rates in the wall jet region as shown in the local Nusselt number distributions.

4. Conclusions

The effects of nozzle exit configuration on turbulent heat transfer enhancements were experimentally investigated for an axisymmetric submerged air jet impinging normal to a heated flat plate. Three orifice nozzles having different nozzle exit configuration, the sharp-edged, standard edged and square-edged nozzle, were tested in this study. In the stagnation region, the sharp-edged orifice jet yields significantly higher heat transfer rates than either the standard-edged orifice jet or square-edged orifice jet. The stagnation point Nusselt number was correlated with the jet Reynolds number and the nozzle-to-plate spacing as $Nu_0 \propto Re^{0.573}(L/D)^{-0.116}$, $Nu_0(Re^{0.571}(L/D)^{-0.092}$, and $Nu_0 \propto Re^{0.566}(L/D)^{-0.078}$, for the sharp-edged, standard edged and square-edged orifice jet, respectively.

For the nozzle-to-plate spacing of $L/D = 2$, the stagnation point Nusselt numbers of orifice jets are nearly 25–55% higher than those of fully-developed pipe jet and approximately 50–75% higher than those of contoured nozzle jet. These heat transfer enhancements are attributed to the large velocity gradient and high turbulence intensity of the orifice jets. The variation in nozzle exit configuration alters the initial flow structure at the nozzle exit, and hence influences on the local heat transfer characteristics.

Consequently, the nozzle exit configuration can be used as an effective passive control technique for heat transfer enhancement. Among three orifice nozzles tested in present study, the sharp-edged orifice nozzle gives the highest local and average heat transfer rates in the stagnation region.

Acknowledgements

This study was supported by Advanced Fluids Engineering Research Center (AFERC), POSTECH.

References

[1] H. Martin, Heat and mass transfer between gas jets and solid surfaces, Advances in Heat Transfer 13 (1977) 1–60.
[2] R. Viskanta, Heat transfer to impinging isothermal gas and flame jets, Exp. Thermal Fluid Sci 6 (1993) 111–134.
[3] R. Gardon, J.C. Akfirat, The role of turbulence in determining the heat transfer characteristics of impinging jets, Int. J. Heat Mass Transfer 8 (1965) 1261–1272.
[4] C.J. Hoogendoorn, The effects of turbulence on heat transfer at a stagnation point, Int. J. Heat Mass Transfer 20 (1977) 1333–1338.
[5] N.T. Obot, A.S. Majumdar, W.J.M. Douglas, The effect of nozzle geometry on impingement heat transfer under a round turbulent jet, ASME Paper No.79-WA/HT-53, 1979.
[6] C.O. Popiel, L. Boguslawski, Effect of flow structure on the heat or mass transfer on a flat plate in impinging round jet, in: Proc. 2nd UK National Conference on Heat Transfer, University of Strathclyde, vol. 1, 1988, pp. 663–685.
[7] Y. Pan, J. Stevens, B.W. Webb, Effect of nozzle configuration on transport in the stagnation zone of axisymmetric impinging free surface liquid jets: Part II — local heat transfer, J. Heat Transfer 114 (1992) 880–886.
[8] K. Oyakawa, T. Azama, I. Senaha, M. Hiwada, Effects of nozzle configuration on impingement heat transfer, in: Proc. 1995 ASME/JSME Thermal Engineering Conference, Maui, USA, vol. 1, 1995, pp. 377–384.

[9] J. Lee, S.J. Lee, Stagnation region heat transfer of a turbulent axisymmetric jet impingement, Exp. Heat Transfer 12 (1999) 139–156.
[10] J. Lee, S.-J. Lee, The effect of nozzle aspect ratio on stagnation region heat transfer characteristics of elliptic impinging jet, Int. J. Heat Mass Transfer 43 (2000) 555–575.
[11] J. Lee, Enhancement in turbulent heat transfer characteristics for jet impingement based on nozzle geometry, Ph.D. Dissertation, Pohang University of Science and Technology, Korea, 1999.
[12] S.J. Kline, F.A. McClintock, Describing uncertainties in single-sample experiments, Mechanical Engineering 75 (1953) 3–8.
[13] F. Hussain, H.S. Husain, Elliptic jets. Part 1. characteristics of unexcited and excited jets, J. Fluid Mech 208 (1989) 257–320.
[14] S.J. Lee, S.J. Baek, The effect of aspect ratio on the near-field turbulent structure of elliptic jets, Flow Meas. Instrum 5 (1994) 170–180.
[15] J. Kestin, P.F. Maeder, H.E. Wang, Influence of turbulence on the transfer of heat from plates with and without a pressure gradient, Int. J. Heat Mass Transfer 3 (1961) 133–154.
[16] R.J. Goldstein, M.E. Franchett, Heat transfer from a flat surface to an oblique impinging jet, J. Heat Transfer 110 (1988) 84–90.